Covalency in La_2CuO_4: A study of ^{17}O hyperfine couplings in the paramagnetic phase

R. E. Walstedt* and S-W. Cheong
Department of Physics, Rutgers University, Piscataway, New Jersey 08855
(Received 5 January 2001; published 5 June 2001)

^{17}O nuclear magnetic resonance spectra from single crystals of La_2CuO_4 are reported for temperatures ranging from 285 to 800 K. Hyperfine tensor data for the planar sites are analyzed using a spin Hamiltonian model that includes spin-orbit coupling effects. The results show a 7.7% hybridization effect of the oxygen $2p_\sigma$ orbital from a single copper neighbor, in good agreement with recent density-functional (DF) calculations by Hüsser *et al.* (HSSM). A large, positive isotropic shift component is also reported, presumably originating from the contact interaction with a hybridized $2s$ orbital component. First-order quadrupolar-splitting data lead to complete characterization of the electric-field gradient (EFG) tensor, which varies only slightly with temperature up to 800 K. EFG tensors for both doped and undoped La_2CuO_4 are fitted with a two-component model, which incorporates a substantial anisotropy in $\langle r^{-3}\rangle$ for the $2p_\sigma$ wave functions, an effect that originated in the DF calculations of HSSM. This analysis reveals an increased charge density on the planar oxygens for the superconducting phase, in accord with the original Zhang-Rice model. However, the increase is found to correspond to only ~80% of the nominal doped-hole density, corroborating a similar conclusion reached recently by Hammel *et al.* Regarding the anomalous spin HF interaction reported in a previous paper for the weakly ferromagnetic state, the present results show that its effects extend all the way to and slightly beyond the orthorhombic-tetragonal phase boundary ($T_{O-T} \simeq 550$ K). Further, the predominant $2s$ contact HF interaction reported here supports the notion, suggested earlier, that a $2s$ admixture underlies the anomaly. However, the basic mechanism of the anomaly remains obscure.

DOI: 10.1103/PhysRevB.64.014404 PACS number(s): 76.60.−k, 75.30.−m, 74.72.Dn

I. INTRODUCTION

In this paper we report and interpret ^{17}O hyperfine (HF) coupling data for the paramagnetic state of La_2CuO_4 (LCO). This compound and its derivatives have an extraordinarily rich history of physical effects. After early prominence as the host compound of the first cuprate superconductor to be refined and identified,[1] LCO went on to become a model system for the quadratic layer, $S=\frac{1}{2}$ antiferromagnet.[2] As such, its magnetic and nuclear magnetic resonance (NMR) properties[3–9] have been successfully compared with first-principles theories.[10] Subsequently, the conditions for such an ideal system have been found to be even more precisely met by the tetragonal-symmetry compound $Sr_2CuO_2Cl_2$ (SCOC),[11] which admits of neither the orthorhombic distortion nor the complicating factor of Dzialoshinsky-Moriya (DM) exchange[12] exhibited by LCO. We shall have occasion to compare our LCO results in this paper with recent work on SCOC.[13]

The DM exchange in LCO gives rise to weak ferromagnetism and has a surprisingly strong influence on the high-field magnetic properties. The resulting body of magnetic effects has received extensive treatment in the literature.[4–6,14,15] There have also been extensive ^{63}Cu NMR and nuclear quadrupole resonance (NQR) studies of LCO,[8,9] but rather less emphasis on ^{17}O. In a recent paper we reported some anomalous ^{17}O shift effects connected with the weakly ferromagnetic state of this compound[16](WCSG). Most pointedly, there is a dramatic change in the ^{17}O HF tensor between the paramagnetic and ordered phases, which is not understood. We shall discuss this phenomenon again below in the light of results presented in this paper.

In its doped, superconducting form, LCO again became a model system, particularly for normal-state magnetic properties. This came about, because the availability of high-quality single crystals led to a uniquely thorough characterization of the dynamic susceptibility component $\chi''(\boldsymbol{q},\omega)$ over wide ranges of $\boldsymbol{q}$, energy, and temperature for $La_{1.85}Sr_{0.15}CuO_4$.[17–19] The neutron results would then appear to form the basis for a comprehensive discussion of the nuclear spin-lattice relaxation time T_1 for $^{63,65}Cu$ and ^{17}O, which are related to $\chi''(\boldsymbol{q},\omega)$ through the fluctuation-dissipation theorem.[20] These matters have been discussed at some length in previous papers.[21,22] The surprising result is that, contrary to calculated estimates, the ^{17}O T_1 process is clearly unrelated to the neutron-determined $\chi''(\boldsymbol{q},\omega)$. It may arise from a ''flat'' term in $\chi''(\boldsymbol{q},\omega)$ which cannot be resolved in neutron studies. There are other NMR effects in the LCO-derived systems, such as the anomalously small indirect spin-spin coupling, which are also related to the ^{17}O HF coupling and are not yet well accounted for.[23]

In spite of the wide-ranging body of ^{17}O NMR studies on LCO-related compounds, there had been, until recently, no investigation of the transferred ^{17}O HF couplings for the case of undoped LCO.[24] Not only are such measurements a foundation for our understanding of the doped cases mentioned above, we shall see that they also provide a quantitative measure of the extremely strong Cu-O hybridization effects in this system. In this paper we compare the latter results with recent density functional (DF) calculations of hybridization and other hyperfine effects on cluster models of LCO carried out by Hüsser *et al.*[25] (HSSM). We also report data for the planar ^{17}O quadrupolar-splitting tensor in the paramagnetic region. Electric-field gradient (EFG) tensor results for the doped and undoped cases are compared and analyzed in conjunction with the HSSM calculations to obtain an estimate of the mobile hole density in the superconducting phase. In accord with the original Zhang-Rice[26]

model of itinerant hole states in the cuprates, we find the bulk of doped-in holes to reside on the planar oxygens. Finally, with the aid of a detailed analysis of susceptibility results, we are also able to extrapolate values for the planar ^{17}O chemical shift tensor. These are compared with results from the literature for $YBa_2Cu_3O_7$.

In Sec. II we describe the methodology of the measurements and present the experimental data. In Sec. III we present a refined model of the HF effects at the planar ^{17}O sites based on spin Hamiltonian methods as discussed, e.g., in the comprehensive summary of these methods by Abragam and Bleaney[27] (AB). We then interpret the data of Sec. II in terms of *s*- and *p*-like covalent admixtures and perform a detailed analysis of EFG tensor results for doped and undoped LCO. A review of the analysis of susceptibility data into spin and orbital components is given, forming the basis for extracting the HF coupling tensor and for extrapolating the chemical shift components. In Sec. IV we summarize the results obtained and discuss their implications for the dramatic transformation which the ^{17}O HF tensor exhibits in the weakly ferromagnetic phase of LCO. Finally, we comment on the doped-phase relaxation anomalies.

II. EXPERIMENTAL METHODS AND RESULTS

A. Methodology

^{17}O NMR spectra were taken on two single crystals of La_2CuO_4, with essentially indistinguishable results, where a one-to-one comparison could be made. The crystals were grown in a CuO flux. Crystal quality is attested to by the narrow and well-defined ^{17}O spectral NMR components for all crystal orientations, both in this paper and in that published earlier.[16] Two annealing procedures were necessary to prepare the crystals for ^{17}O NMR studies. First, they were annealed for 3 days at 900°C in ~ 0.8 Atm of O_2 gas containing $\sim 50\%$ of the ^{17}O isotope. This brings about a complete exchange of the enriched isotope mixture into both oxygen sites of the crystal. Following that, it was necessary to remove a slight excess of oxygen by annealing overnight in a closed, evacuated manifold at $T \sim 590$°C. This procedure was found to yield $T_N > 310$ K,[16] close to the upper limit of $T \sim 325$ K, which corresponds to exact stoichiometry.[4,5]

Once ''exchanged,'' a given crystal tended to lose its elevated concentration of ^{17}O at high temperatures, evidently by means of a process of chemical exchange with O_2 molecules in the atmosphere surrounding the sample. At the highest temperatures employed, this process would take place on a time scale ~ 1 h. To prevent this, the experimental NMR furnace was purged with He gas before a run was started, then a very tiny overpressure of He was maintained while the furnace was at an elevated temperature. In this way, loss of ^{17}O during the logging of NMR data was rendered negligible.

NMR spectra were taken using a spin-echo Fourier transform method with quadrature detection. An ^{17}O spectrum taken this way at $T = 400$ K with the field $H_0 (\sim 7.3$ T) lying in the ab (i.e., CuO_2) plane is shown in Fig. 1. The crystal is oriented so that the field is either $\parallel$ or $\perp$ to the local

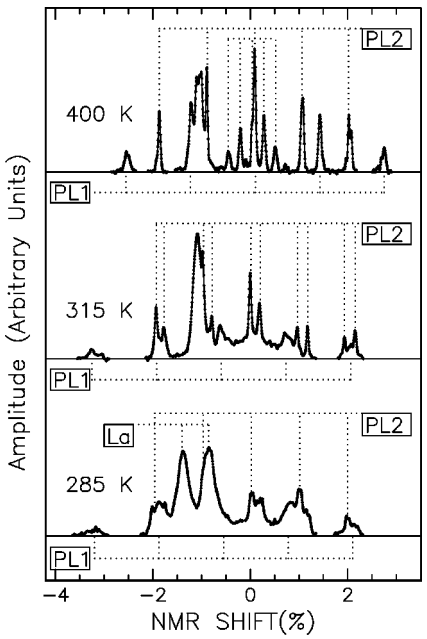

FIG. 1. ^{17}O NMR spectra taken on a single crystal of La_2CuO_4 at three temperatures as described in the text. The crystal is oriented so that the field lies along the *a* and *b* axes of the crystal which, with twinning, will have equal probability. Three quintets of ^{17}O NMR lines are delineated using dotted lines. ''PL1'' and ''PL2'' are planar sites with the field parallel and perpendicular to the bond axis, respectively. The apical sites yield a closely spaced quintet near zero shift. The large feature near -1% is a quadrupolar satellite of the ^{139}La spectrum. The complex behavior with temperature is discussed in the text.

Cu-O-Cu bond axis for the planar ^{17}O sites. The latter sites each yield a uniformly spaced quintet of lines with different shifts and quadrupolar interactions (labeled PL1 and PL2 in Fig. 1). Another quintet of lines with a much smaller spectral width is seen near the center of the pattern. This group of lines corresponds to the apical sites, which are much more weakly coupled with the unpaired spins of the Cu^{2+}. We shall ignore the effects of these sites in the present paper. Another feature visible at a shift of $\sim -1\%$ is a quadrupolar satellite line from the ^{139}La spectrum.[16] This line becomes less intense at higher temperatures and did not pose a problem for the measurement of shifts and quadrupolar parameters, which was accomplished by measuring the satellite line frequencies. Also, the splitting of the PL2 line components visible at low temperatures in Fig. 1 is negligible at $T = 500$ K and above.

The HF coupling anomaly reported in WCSG is clearly visible in the lower two panels of Fig. 1. There, the quintets have been identified assuming that the quadrupolar splittings remain fixed at their high-temperature values. At 315 K ($T \simeq T_N$) one sees that the PL1 (bond axis) component has moved to a substantially negative shift value from its ~ 0 value at 400 K. The PL1 shift decreases further at 285 K, where the lines have also become smeared out. Similar behavior is observed with field along the *c* axis.[16] Meanwhile, PL2 splits into two rather sharp peaks at $T \sim T_N$, then also smears out at 285 K, *but remains essentially unshifted*. The

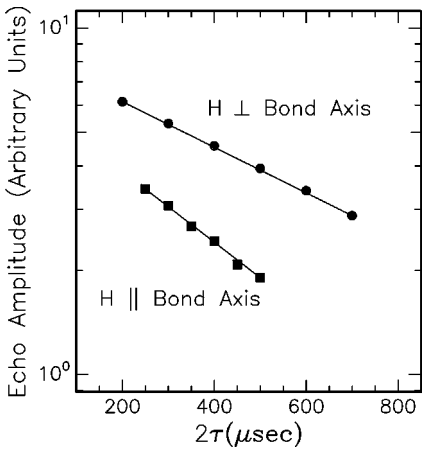

FIG. 2. ^{17}O spin-echo decay data are plotted semilogarithmically for two in-plane orientations of the field for the $\pm\frac{1}{2}\leftrightarrow\pm\frac{3}{2}$ transition at $T\sim 400$ K. The contrast in exponential decay rates is analyzed in the text. It is taken as evidence that ''PL1'' and ''PL2'' (Fig. 1) correspond to field orientations parallel and perpendicular to the bond axis, respectively.

surprising conclusion is that near $T\sim T_N$, the planar oxygen HF tensor (a) reverses its sign, (b) becomes enhanced by well over an order of magnitude, and (c) exhibits $\sim 100\%$ anisotropy. These characteristics do not correspond to any known HF mechanism, but are somewhat reminiscent of the functional form of DM exchange coupling.[14] As far as we are aware, such an effect has not yet been reported for any other system. We comment further on the HF anomaly in Sec. IV.

B. Site verification using T_2

It was argued in WCSG that the spectrum labeled PL1 (Fig. 1) corresponds to field orientation along the Cu-O-Cu symmetry axis. However, since the EFG tensor deviates strongly from axial symmetry, we have sought to verify the site identification with a simple T_2 measurement. The spin-echo T_2 processes for the PL1 and PL2 satellites are expected to be dominated by T_1-modulated dipolar couplings with the two nearest-neighbor $^{63,65}Cu$ nuclear spins, for which we expect[23] an exponential decay with

$$1/T_2=\langle\Delta\omega^2\rangle T_{1\mathrm{Cu}}, \tag{1}$$

where $\langle\Delta\omega^2\rangle$ is the unlike-spin ^{17}O second moment and T_{1Cu} is the $^{63,65}Cu$ T_1, which we treat approximately as a single parameter.[28] The spin echo T_2 decay data are shown in Fig. 2, where they are seen to be very nearly exponential. Since the ratio of axial to transverse dipolar fields is 2, the ratio of $\langle\Delta\omega^2\rangle_\parallel$ to $\langle\Delta\omega^2\rangle_\perp$ is 4, and since the T_1 parameter [Eq. (1)] is the same for both, the T_2 value for the orientation parallel to the Cu-O-Cu bond axis is expected to be $\frac{1}{4}$ that of the perpendicular orientation. We therefore identify the shorter (PL1) T_2 value as the bond axis orientation, as before. The fact that the experimental ratio of T_2 values is 1.9 rather than 4 we take as evidence for a small indirect spin-spin coupling adding to the dipolar contribution. An indirect coupling about half of what was calculated for the Sr-doped LCO case[23] would account for this discrepancy.

It is interesting to make a quantitative estimate of T_2 using Eq. (1). For the case of $\boldsymbol{H}\perp$ bond axis, we find $\langle\Delta\omega^2\rangle_\perp = 3.9\times 10^7$ s^{-2} with dipolar couplings[29] and NQR $T_1 \simeq 125$ μs at $T=435$ K.[8,9] Equation (1) then gives $T_2 \simeq 200$ μs, compared with the measured value of 428 μs (Fig. 2). Since the indirect coupling probably enlarges $\langle\Delta\omega^2\rangle_\perp$, the slowing of the experimental T_2 in this case is probably due to the anisotropy of T_1. The NQR T_1 value quoted is for a quantization axis $\perp CuO_2$ planes, whereas the in-plane value required here is probably shorter by a factor of $2\rightarrow 3$.[30] Such an effect would bring the foregoing estimate much closer to the experimental value.

C. Shift and quadrupolar tensor data

Satellite line position data were recorded for the planar oxygen site over temperatures ranging from 400 to 800 K in a field of 7.3 T. Analysis of these data yielded a complete characterization of the NMR shift and quadrupolar interaction tensors over the stated temperature range. In this section we describe the methodology used to record line frequency data and extract from it the relevant physical parameters.

In the LCO structure the three mutually orthogonal principal axes of the shift and EFG tensors lie along the symmetry axes of the crystal. The resonance frequency $\nu_{R\alpha}$ of any member of the ^{17}O ($I=\frac{5}{2}$) quintet of lines can be expressed

$$\nu_{R\alpha}=\nu_{L\alpha}\pm N_1\nu_{Q\alpha}+N_2(\nu_{Q\beta}-\nu_{Q\gamma})^2/\nu_{L\alpha}, \tag{2}$$

where $N_1=0,1$, and 2 for the $(\frac{1}{2}\leftrightarrow-\frac{1}{2})$, $(\pm\frac{1}{2}\leftrightarrow\pm\frac{3}{2})$, and $(\pm\frac{3}{2}\leftrightarrow\pm\frac{5}{2})$ transitions, respectively, and $N_2=\frac{2}{9}$, $\frac{5}{36}$, and $-\frac{1}{9}$ for the same respective transitions.[31] The subscripts α, β, and γ refer to Cartesian axes, where α is the direction of the applied field, and $\nu_{Q\alpha,\beta,\gamma}$ are the three first-order quadrupolar frequency parameters. $\nu_{L\alpha}=\gamma H(1+K_\alpha)$ is the nuclear Larmor frequency with the field along the α axis. We note that the second-order corrections in Eq. (2) are of order 1 kHz and are barely resolved within the precision of the measurements.

Typically, data for the $\nu_{R\alpha}$ were extracted from the measured beat frequencies of a pair of noise-averaged free-induction signals spaced by ~ 15 kHz on either side of $\nu_{R\alpha}$. This method was found to be superior in accuracy to spin-echo Fourier transform spectra. The field H was measured with an ^{17}O-doped H_2O probe. Most of the data were obtained using pairs of $(\pm\frac{1}{2}\leftrightarrow\pm\frac{3}{2})$ satellite lines, resulting in shift components K_α accurate to ~ 10 ppm. Using Eq. (2), pairs of satellite frequencies can be immediately combined to yield the $\nu_{Q\alpha}$ and estimates of the $\nu_{L\alpha}$. The latter can then be employed to determine the second-order shifts. Iterating this process yields final numbers for all parameters very quickly.

Quadrupolar frequency parameters $\nu_{Q\alpha}$ $(\alpha=a,b,c)$[32] were measured at a series of temperatures in the paramagnetic region. The $\nu_{Q\alpha}$'s were very nearly constant in the range 500 K$\leqslant T\leqslant$800 K, with measured values and error limits given in Table I. The results were found to obey

TABLE I. ^{17}O NQR splitting ($\nu_{Q\alpha}$), g factor (g_α), temperature derivative of shift (dK_α^{expt}/dT) and susceptibility ($d\chi_\alpha/dT$) data, and the shift coefficient (β_α) are all tabulated. Also shown are the extrapolated chemical shift values (K_α^{ch}) from Fig. 4 and literature values (Ref. 31) for YBCO ($K_{\alpha YBCO}^{ch}$) for comparison. The units of the parameters shown are $\nu_{Q\alpha}$, MHz; $dK_\alpha/dT, 10^{-7}\mathrm{K}^{-1}$; $d\chi_\alpha/dT, 10^{-8}$(emu/mol K); β_α,(emu/mol)$^{-1}$; K_α^{ch}, %. Parentheses show uncertainty in the last decimal place.

α	g_α	$\nu_{Q\alpha}$	$\nu_{Qd\alpha}$	dK_α/dT	$d\chi_\alpha/dT$	β_α	K_α^{CH}	$K_{\alpha\mathrm{YBCO}}^{\mathrm{CH}}$
b	2.077	0.574(3)	0.69(3)	12.4(4)	7.95	15.6(5)	0.056(7)	0.066(10)
a	2.077	−0.427(3)	−0.47(2)	5.9(6)	7.95	7.4(7)	0.036(9)	0.02(1)
c	2.308	−0.147(3)	−0.22(2)	3.8(5)	9.82	3.9(5)	0.027(10)	0.02(3)

Laplace's equation, giving $\Sigma_\alpha \nu_{Q\alpha}=0$ within estimated error limits, helping to validate the accuracy of crystal orientations used. The tabulated values yield an asymmetry factor $\eta=0.49\pm0.01$. Also shown in the table are literature values $\nu_{Qd\alpha}$ for doped, superconducting LCO (Ref. 33) (IKZA). The effect of doping is seen to be a ~20% increase in the principal component and a decrease in the asymmetry factor to $\eta_d=0.36$. In Sec. III we use a model calculation of EFG components to analyze and discuss the EFG tensor data for both doped and undoped LCO.

The NMR shift data for the planar sites are plotted vs T in Fig. 3, along with c-axis values for the apical site shift. The latter serve as a fiduciary against which we can contrast the marked influence of the weakly ferromagnetic phase transition on the planar site shifts. Below ~600 K, the shift values begin to be affected by the approaching transition to the ordered magnetic phase, which occurs at $T\sim300$ K, by which point the a and b axis shift values become sharply negative (see Fig. 1 and Ref. 16). Above $T=600$ K the behavior of the $K_\alpha(T)$ is linear within the scatter of the data, as is the behavior of the measured susceptibility $\chi_\alpha^{\mathrm{expt}}(T)$ ($\alpha=b,ac$) for 500 K$\leqslant T\leqslant$800 K.[34] We take the slopes of the least-squares linear fits to the data shown in Fig. 3 and to that in Ref. 34 to be proportional to the spin paramagnetic components of shift and susceptibility, respectively. The ^{17}O spin shift coefficients β_α^s are then extracted from these fits using

$$\beta_\alpha^s=\frac{K_\alpha^s}{\chi_\alpha^s}=\frac{dK_\alpha^{expt}/dT}{d\chi_\alpha^{expt}/dT}. \tag{3}$$

Finally, we obtain the hyperfine coefficients $C_\alpha=g_\alpha\beta_\alpha\mu_B N_A/2$, where g_α is the electronic g factor, and we remind the reader that C_α is defined by the HF coupling Hamiltonian written $\mathcal{H}_{HF}=\Sigma_\alpha C_\alpha I_\alpha S_\alpha$.[35] Values of g_α are extracted from the susceptibility data, where we take $g_c^2/g_{ab}^2=(d\chi_c^{expt}/dT)/(d\chi_{ab}^{expt}/dT)$ for temperatures well above the ordered phase. We adopt the expressions

$$g_c=2(1+4|\lambda|/\Delta_0);\quad g_{ab}=2(1+|\lambda|/\Delta_1), \tag{4}$$

where λ is the spin-orbit coupling parameter and the $\Delta_{0,1}$ are the crystal-field splitting energies to the $d_{xy}, d_{yz,zx}$ excited states, respectively. In this discussion we shall neglect the small difference between Δ_0 and Δ_1[36] (see also Sec. III A below). With the experimental ratio $g_c/g_{ab}=1.111$ and Eq. (4), one finds $g_c=2.308$ and $g_{ab}=2.077$.

Using the data in Table I in the formulas of the previous paragraph, we obtain the HF tensor (C_α^{expt}) for La_2CuO_4. C_α^{expt} values are presented along with data[21] for $La_{1.85}Sr_{0.15}CuO_4$ (labeled $C_{d\alpha}^{expt}$) in Table II. In Sec. III the HF tensors are corrected for direct dipolar couplings and analyzed into isotropic and anisotropic components using the formulas $C^{iso}=\frac{1}{3}\Sigma_\alpha C_\alpha$ and $C_\alpha^{an}=C_\alpha-C^{iso}$. We note here that this procedure yields $C^{iso}=52$ kG/spin and $C_d^{iso}=83$ kG/spin, a roughly 60% increase with doping. In Sec. III these points will be discussed further, along with a more detailed analysis.

Finally, it is interesting to contrast the values of C_α in Table II with similar data reported for SCOC.[13] There, for example, the bond axis value is given as 83 ± 7 kG/μ_B, which is approximately twice the bond axis value we find for

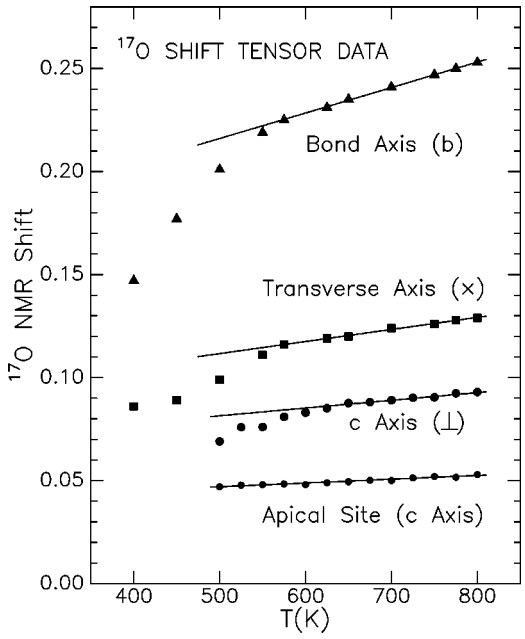

FIG. 3. Planar ^{17}O NMR shift data are plotted as a function of temperature T for all three orientations of the crystal axes. The ''transverse axis'' refers to the a axis. Also shown are data for the apical site with field along the c axis. Noting that the susceptibility data (Ref. 32) vary linearly with T in this range, deviations from this behavior for the planar oxygens signal the onset of a dramatic change in the HF tensor in the magnetically ordered state. Interestingly, the a axis shift shows the onset of a change below 600 K here, but at lower T, its change is very small compared with that for the b and c axes.

TABLE II. ^{17}O HF coefficients C_α defined and discussed in the text are tabulated in units of kG/spin. Quantities relating to the doped case are subscripted ''$d\alpha$.'' These are taken from Ref. 16. Parentheses show uncertainty in the last decimal place.

α	$C_{d\alpha}^{expt}$	C_α^{expt}	C_α^{dip}	$C_{d\alpha}^{corr}$	C_α^{corr}	$C_{d\alpha}^{an}$	C_α^{an}	C_α^{σ}	C_α^{π}
b	108(16)	90(3)	10.1	98	80(3)	15	27.6	32.2	−4.6
a	77(11)	43(4)	−2.4	79	45(4)	−3	−6.9	−16.1	9.2
c	64(10)	25(3)	−6.6	71	32(3)	−12	−20.7	−16.1	−4.6

LCO, given that the HF field per unit of spin[35] will be larger than the (kG/μ_B) figure quoted by a factor $g_{ab}\sim 2$. The other components for SCOC are correspondingly large, giving a remarkable contrast in the HF parameters for two so similar compounds. We feel that this result should be carefully checked before accepting it as fact.

III. THEORY AND INTERPRETATION OF RESULTS

In this section we present a cooordinated discussion of the HF and EFG tensors for the planar oxygen sites, using both the La_2CuO_4 data presented in this paper and $La_{1.85}Sr_{0.15}CuO_4$ data from the literature. The HF and EFG tensors are closely related in principle and in practice. These quantities sense the distributions of spin and charge, respectively, and, furthermore, both depend on values of $\langle r^{-3}\rangle$ for on-site occupied orbitals as well as $1/r^3$ lattice sums for contributions from more distant sites. Using the HSSM DF calculations as a basis for the local contributions, we find below a remarkable contrast in behavior between the HF and EFG parameters.

A. Ligand HF coupling formulas

The theory of HF couplings for ionic states in solids and their associated ligands is a subject that has received considerable attention in the past. Thus, we can present what is expected to be a relatively complete formulation of expected NMR shift behavior at the planar oxygen sites in LCO in terms of the spin Hamiltonian approach employed in AB. While the general formulation given is applicable to oxygen, there is not a ready-made set of formulas for the case of ^{17}O HF effects on O^{2-} ligands in the literature. This is because ^{17}O is a rare isotope and did not figure in EPR hyperfine effect studies, for which the theory was originally worked out.

In the following we shall develop formulas for the planar ^{17}O case using the methods that were used extensively in the literature and have been summarized by AB. Particularly useful were the methodologies described in Chaps. 17 and 20 of that volume. However, it must be noted in advance that AB treat only impurity states using perturbation methods. Therefore, the inherent symmetry of a complete lattice of magnetic ions is not taken account of. This will undoubtedly give rise to quantitative errors owing to the high levels of hybridization found to be present in this system. The more advanced techniques used, e.g., by HSSM, may incorporate effects unforeseen in our approach. Nonetheless, we feel that the formulas employed here give a sufficiently general framework so that all significant effects can be represented, even though their underlying physical mechanism may remain obscure.

With the foregoing methods, the spin-paramagnetic ground-state hyperfine expression becomes

$$\mathcal{H}_G^s = 2C^{iso}\vec{I}\cdot\vec{S} + 2\sum_\alpha C_\alpha^{an} I_\alpha S_\alpha , \tag{5}$$

where the HF coefficients, defined for a single Cu neighbor, are given by $C_b^{an}=(2f_{p\sigma}+\frac{1}{2}f_{SO}f_p')\alpha_p$; $C_c^{an}=-(f_{p\sigma}+\frac{7}{2}f_{SO}f_p')\alpha_p$; $C_a^{an}=-(f_{p\sigma}-3f_{SO}f_p')\alpha_p$; and $C^{iso}=\alpha_s f_s - 5\alpha_p f_p' f_{SO}$. In the latter expressions, $\alpha_{s,p}$ are hyperfine constants discussed below, and the $f_{s,p\sigma}$ are so-called ''spin densities'' giving the statistical weight of the hybridized wave function residing in ligand orbitals of s and p_σ character, respectively.[27] Further, $f_{SO}=|\lambda|(N_t N_\sigma)^{-\frac{1}{2}}/\Delta$, where λ is the spin-orbit coupling parameter, Δ is an average crystal-field splitting parameter,[36] and N_σ and N_t are hybrid wave-function normalization factors for the ground and excited states, respectively.[37] $f_{p\sigma}$ and f_p' are closely related parameters.[38] In practice we shall not distinguish between them. Regarding Eq. (5), we note that if f_{SO} were zero, this would simply be a first-order combination of contact and dipolar hyperfine terms proportional to the s- and p-like spin transfer, respectively, onto the oxygen sites. The second-order terms are very similar to those which occur on the Cu^{2+} site.[39] They upset the axial symmetry of the dipolar term around the Cu-O-Cu bond direction, thus resulting in a small contribution to the isotropic HF term.

The two basic hyperfine constants in $\mathcal{H}_G^s$ are $\alpha_p = \frac{4}{5}\hbar\gamma_{17}\mu_B\langle r^{-3}\rangle_p$ for the dipolar terms and the corresponding s-contact HF coefficient α_s, which requires special comment. The traditional contact HF coefficient is given by $\alpha_s = \frac{16}{3}\pi\hbar\gamma_{17}\mu_B|\Psi_{2s}(0)|^2$, representing the effect of a partial hole occupation of the $2s$ shell of the oxygen. The work of HSSM has suggested that a strong isotropic HF coupling is present (consistent with experiment), without identifying the specific mechanism responsible for it. Since the well-known core-polarization mechanism would in this instance almost certainly give a negative shift, we suggest that a small $2s$ hybridization must be at work here. We discuss this point further in the comparison with experimental data below. In order to compare the data of Sec. II with Eq. (5), we require expressions for the corresponding shift coefficients $\beta_\alpha = K_\alpha^s/\chi_\alpha^s$. These are

$$\beta_b = 2[\alpha_s f_s - 5\alpha_p f_{p\sigma} f_{SO} + \alpha_p f_{p\sigma} \times (2 + \tfrac{1}{2} f_{SO})]/(N_A \hbar \gamma_{17} g_{ab} \mu_B), \quad (6)$$

$$\beta_a = 2[\alpha_s f_s - 5\alpha_p f_{p\sigma} f_{SO} - \alpha_p f_{p\sigma} \times (1 - 3 f_{SO})]/(N_A \hbar \gamma_{17} g_{ab} \mu_B), \quad (7)$$

$$\beta_c = 2[\alpha_s f_s - 5\alpha_p f_{p\sigma} f_{SO} - \alpha_p f_{p\sigma} \times (1 + \tfrac{7}{2} f_{SO})]/(N_A \hbar \gamma_{17} g_c \mu_B). \quad (8)$$

B. The anisotropic shift

We begin by correcting $C_{d\alpha}^{expt}$ and C_{α}^{expt} in Table II for direct dipolar hyperfine coupling. The dipolar field due to a moment $\vec{\mu}_i$ located at r_i with respect to the target planar oxygen site is given by $\vec{H}_i^d = 3\vec{r}_i(\vec{\mu}_i \cdot \vec{r}_i)/r_i^5 - \vec{\mu}_i/r_i^3$. The dipolar coupling tensor C_{α}^{dip} is the sum of field components in the α direction with the $\vec{\mu}_i$ polarized in that direction, per unit of spin contained in a unit cell. Owing to hybridization, the spin polarization is physically divided between the copper and planar oxygen sites. For uniform polarization we have $\mu_{i\alpha} = g_\alpha \mu_B \langle S_\alpha \rangle_i$. In terms of the hybridization parameter $f_{p\sigma}$, then

$$C_{\alpha}^{dip} = (1 - 4f_{p\sigma}) g_\alpha \mu_B \sum_{i(Cu)} (2x_{i\alpha}^2 - x_{i\beta}^2 - x_{i\gamma}^2)/r_i^5 + 2 f_{p\sigma} g_\alpha \mu_\beta \sum_{j(O)} (2x_{i\alpha}^2 - x_{i\beta}^2 - x_{i\gamma}^2)/r_i^5, \quad (9)$$

where (α, β, γ) are cyclical and the two sums are on copper and oxygen sites, respectively. These sums have been carried out with the results given in Table II. The demagnetizing contribution, which is <1 kG/spin, has been included in these results by summing over a volume with the approximate shape of the sample. Subtracting C_{α}^{dip} from the experimental data then leads to the corrected (i.e., local) HF tensors C_{α}^{corr} and $C_{d\alpha}^{corr}$ in Table II. The anisotropic portion of the latter tensors is obtained using the formulas given at the end of Sec. II C, and are tabulated as C_{α}^{an} and $C_{d\alpha}^{an}$. These quantities can now be compared with the local HF tensor formulation of Sec. III A.

As noted earlier, there is substantial and unexpected HF anisotropy around the bond axis. To facilitate the discussion of this effect, we further divide the anisotropic term C_{α}^{an} into σ-like and π-like components using $C_{\alpha}^{an} = C_{\alpha}^{\pi} + C_{\alpha}^{\sigma}$, where $(C_a^{\pi}, C_b^{\pi}, C_c^{\pi}) = (2s, -s, -s)$ and $(C_a^{\sigma}, C_b^{\sigma}, C_c^{\sigma}) = (-r, 2r, -r)$. From the parameters in Eq. (5) we have $s = \frac{13}{6} f_{SO} f_p' \alpha_p$ and $r = f_{p\sigma}\alpha_p + \frac{4}{3} f_{SO} f_p' \alpha_p$. Experimental values for the C_{α}^{π} and C_{α}^{σ} tensors are shown in Table II. Both terms are clearly resolved. There is a similar effect for $C_{d\alpha}^{an}$, but we omit further discussion on account of the large error bars.

We first analyze the p_σ contribution, which can be written

$$C_{\alpha}^{\sigma} = \alpha_p f_{p\sigma}(1 + 4 f_{SO}/3) = 16.1 \text{ kG/spin}. \quad (10)$$

To evaluate the primary hybridization parameter $f_{p\sigma}$, we develop estimates of both α_p and f_{SO}. In units of kG/spin, we have $\alpha_p = 8 \times 10^{-4} \mu_B \langle r^{-3} \rangle_p$. We use the value $\langle r^{-3} \rangle_p \simeq 4.0$ a.u.[40] This value leads to $\alpha_p = 200$ kG/spin. Next, we obtain an estimate of f_{SO} from the values of the g_α derived earlier (Table I), where we have $g_c \simeq 2(1 + 4 f_{SO})$. With $g_c = 2.308$ we find $f_{SO} \simeq 0.0385$. Substituting the foregoing values for α_p and f_{SO} into Eq. (10) then yields $f_{p\sigma} = 0.077$. This is a high degree of covalency, but is in good agreement with the DF calculated value (0.082) given by HSSM. It means, for example, that 31% of the Cu^{2+} 3d hole actually resides in the p_σ orbitals of the ligands. This is substantially larger than $f_{p\sigma} = 0.0495$ reported for $KNiF_3$.[27] We also note that the p_σ admixture is only a lower limit for the total covalency, since there are the additional effects of f_s [Eq. (5)] and the neglected effects of the apical sites.

In the same way, with $f_p' \simeq f_{p\sigma}$, we have $s \simeq \frac{13}{6} f_{SO} f_p' \alpha_p$. Using parameter values from the previous paragraph, we find $s \simeq 1.5$ kG/spin. This estimate of the p_π component is only one-third the value shown in Table II, and clearly does not account for the data. In this connection, some recent results from HSSM[40] are of interest. They show an anisotropy with the same sense as the experimental result, only somewhat smaller. Adding the second-order correction, we then find marginal agreement with the experimental data in Table II.

C. The contact shift

In Eq. (5) we envisioned the contact HF field as arising from hybridization with the $2s$ orbital. While its origin is not entirely clear, we can compare the HSSM isotropic shift result

$$\frac{8\pi}{3}\left[\sum_m |\Psi_m^{\uparrow}(0)|^2 - \sum_m |\Psi_m^{\downarrow}(0)|^2\right](2\mu_B/a_B^3) = 81.4 \text{ kG/spin} \quad (11)$$

with the corresponding experimental quantity C^{iso} [Eq. (5)]. In Eq. (11) the factor $(2\mu_B/a_B^3)$ (a_B = Bohr radius) converts the HSSM result in a.u. to Gauss/spin. For comparison with experiment, the isotropic HF result in Table I must be corrected [see Eq. (5)] by adding $5\alpha_p f_p' f_{SO} \sim 4$ kG/spin to obtain $\alpha_s f_s \simeq 57$ kG/spin, in only rough agreement with the HSSM result of Eq. (11). This discrepancy is, perhaps, not surprising, because the behavior of closed-shell orbitals may be involved here, and such behavior is notoriously difficult to calculate.

We note several points in connection with the isotropic ^{17}O HF coupling. First, the HSSM result is positive, and is proportional to the number of Cu neighbors. HSSM labeled this a core polarization (CP) HF coupling. The traditional CP mechanism, which would operate through a $2p$ spin density on the oxygen site, would almost certainly give a negative coupling in this case.[42] Thus, the principal isotropic HF effect would appear to be the $2s$ admixture noted earlier. Thus, we are left with the tentative conclusion that the planar oxy-

TABLE III. Experimental data for the EFG tensor given in Sec. II C (Table I) are tabulated along with model tensor components described in the text for the scenario where the local (on-site) components have asymmetry owing to anisotropic values of $\langle r^{-3}\rangle$. Quantities corresponding to the doped case are subscripted ''$d\alpha$.'' All EFG values are given in a.u., where $Q_{17}=0.026$ barns has been used to convert experimental $\nu_{Q\alpha}$ values.

α	$10V_\alpha^{latt}$	V_α^{loc}	V_α^{fit}	V_α^{expt}	$10V_{d\alpha}^{latt}$	$V_{d\alpha}^{loc}$	$V_{d\alpha}^{fit}$	$V_{d\alpha}^{expt}$
b	0.349	0.449	0.621	0.624	0.378	0.624	0.751	0.749
a	−0.284	−0.277	−0.462	−0.464	−0.278	−0.385	−0.515	−0.510
c	−0.065	−0.172	−0.159	−0.160	−0.100	−0.239	−0.236	−0.240

gens undergo a $2s$ admixture proportional to the number of Cu neighbors. Further discussion of this point is given in Sec. IV.

D. Quadrupolar tensor results

As we saw in Sec. II C, the quadrupolar interaction tensor ($\nu_{Q\alpha}$) for LCO deviates strongly from axial symmetry, and is more asymmetric and slightly smaller in magnitude than for the doped case tensor (see Table I). Doping increases hole density in the system, and as the hole carriers are thought to reside primarily on the planar oxygen, a modest increase in $\nu_{Q\alpha d}$ over $\nu_{Q\alpha}$ is expected and is observed. We present here an analysis of the EFG data in which we draw upon some unique features of recent calculations by HSSM.[40] To motivate our point of view, we first review some recent literature.

Relying on calculations by Hanzawa *et al.*,[41] IKZA modeled the planar ^{17}O EFG as entirely local in origin, the anisotropy being generated by charge occupation of p_π orbitals. This approach rested on estimates showing that the EFG contribution from the surrounding lattice is an order of magnitude smaller than the on-site contribution. These authors have used this model extensively to discuss EFG behavior in the cuprates. However, since the HSSM results show that little or no p_π hole density is expected, we prefer to adopt an alternative viewpoint developed by Takigawa *et al.*, for the case of $YBa_2Cu_3O_7$, where the local EFG contribution is derived from an on-site p_σ hole-density combined with an (essentially) point-charge contribution from the surrounding lattice, which is enhanced[31] by an antishielding factor $\xi_\infty = 1-\gamma_\infty \simeq 10$.

For the LCO case, we embellish the latter model with the interesting feature of a *locally anisotropic* EFG contribution. This effect arose unexpectedly from the HSSM DF calculations[40] in the guise of an anisotropy in $\langle r^{-3}\rangle$. As we shall see, it plays an important role in understanding the EFG data. For the lattice contribution we perform a point-charge EFG calculation in which the $2p$ hybridization effects of Sec. III A are taken into account, summing over neighbor sites. Hybridization effects at the apical sites, being of order 1%, are neglected. For the lattice EFG tensor contribution the core summand is $V_{i\alpha}^{latt}=q_i(2x_{i\alpha}^2-x_{i\beta}^2-x_{i\gamma}^2)/r_i^5$, essentially the same as in Eq. (9) except that because of charge neutrality ($\Sigma_i q_i=0$) over the unit cell, the sum on neighbor sites converges quickly. In the doped case we presume that some percentage of the doped holes resides on the oxygen sites, the precise amount being taken as an adjustable parameter. To preserve charge neutrality we place an equal and opposite charge on the La sites. This assumption of doped charge homogeneity is, of course, only an approximation. The results of the point-charge calculation are shown in Table III as $10V_\alpha^{latt}$ and $10V_{d\alpha}^{latt}$, i.e., multiplied by 10 to facilitate comparison with the local contribution and the experimental data.

For the local contribution we employ a simple formula for the principal EFG component, $V_\alpha^{loc}=0.8q_\sigma\langle r^{-3}\rangle_{\sigma\alpha}$ (α=a,b,c), where q_σ is the $2p_\sigma$ hole density per planar oxygen. q_σ/e is taken to be twice the hybridization parameter $f_{p\sigma}$ determined in Sec. III A for the undoped case. For the doped case a variable mobile hole density is added as well, up to a maximum of $0.075e$ per oxygen. The calculated anisotropy of $\langle r^{-3}\rangle_{\sigma\alpha}$ is taken account of by setting $\langle r^{-3}\rangle_{\sigma b}=4.0$ a.u. for the principal component V_b^{loc}, and adjusting V_a^{loc} and V_c^{loc} to give the calculated asymmetry[25,40] $\eta_{loc}=(V_c^{loc}-V_a^{loc})/V_b^{loc}=0.234$, while satisfying LaPlace's equation. η_{loc} is taken to be independent of doping.

We fit this two-component model to the doped and undoped EFG data (Table III) simultaneously with the following least-squares method. Each experimental EFG tensor is represented as $V_\alpha^{fit}=\xi_{loc}V_\alpha^{loc}+\xi_\infty V_\alpha^{latt}$. The total rms error is then minimized by setting the derivatives of

$$\mathrm{MSQ}=\sum_\alpha (V_\alpha^{expt}-\xi_{loc}V_\alpha^{loc}-\xi_\infty V_\alpha^{latt})^2 + \sum_\alpha (V_{d\alpha}^{expt}-\xi_{loc}V_{d\alpha}^{loc}-\xi_\infty V_{d\alpha}^{latt})^2 \qquad (12)$$

with respect to ξ_{loc} and ξ_∞ equal to zero. The resulting pair of linear equations is then solved for ξ_{loc} and ξ_∞. This procedure has been carried out for a series of assumed levels of mobile charge density. At each such level, $V_{d\alpha}^{latt}$ is recalculated with adjusted point-charge values in the lattice. The optimum fit obtained in this way corresponds to 80% charge mobility. The corresponding fitted tensor values are given in Table III, where the antishielding factors found are $\xi_{loc}=0.53$ and $\xi_\infty=11.5$. The value found for ξ_{loc} is rather small, but not outside of the range of calculated values reported in the literature.[43] The value of ξ_∞ is similar to that reported for $YBa_2Cu_3O_7$.[31]

This model EFG tensor fits the results for the doped and undoped cases to ~1% (Table III). We therefore see that the

TABLE IV. Single-crystal susceptibility data for doped and undoped LCO, along with spin and Van Vleck (orbital) components derived from these data as described in the text. The last column gives the reference from which the data are taken. All data were taken in low field, except for that from Ref. 16, which were taken in $5T$. All susceptibilities are in units of 10^{-6} emu/mol. The orientation α indicates field along the c axis or in the ab plane.

Composition	T	α	$\chi_\alpha^{expt}(T)$	$\chi_\alpha^s(T)$	χ_α^{vv}	Ref.
La_2CuO_4	800 K	c	97	138	58	34
		ab	25	112	13	
$La_{1.92}Sr_{0.08}CuO_4$	300 K	c	120	174	45	46
		ab	52	141	10	
$La_{1.85}Sr_{0.15}CuO_4$	300 K	c	135	182	53	21
		ab	60	147	11	
La_2CuO_4	350 K	c	54	45	108	16
		ab	−39	37	24	

measured EFG tensor is at least a semiquantitative measure of the mobile charge density in the superconducting phase. The results indicate that a major fraction of doped holes in the superconducting phase are actually itinerant and reside on the planar oxygen sites. However, a substantial number appear to remain localized, in accord with a recent NQR study and analysis.[44]

E. Review of susceptibility analysis

In Sec. II C the linear variation of both shift and susceptibility enabled us to extract the spin HF coupling in a straightforward and accurate manner. In previous work, this extraction had to rely on *estimates* of the orbital shift and/or susceptibility.[21,16] In this section we take the opportunity to partition the susceptibility of both doped and undoped LCO using single crystal data and a minimum of assumptions. As a consequence, we are able to obtain an experimental measure of the orbital (i.e., chemical) shift tensor for LCO. We then use these data to review and revise some results from earlier papers.

Given the values of the bulk susceptibility $\chi_\alpha^{expt}(T)$ at some temperature T with the field both perpendicular to the CuO_2 planes and lying in these planes, we partition the $\chi_\alpha^{expt}(T)$ into spin, orbital, and core diamagnetic components as follows: First, the core diamagnetic component of susceptibility χ_{dia} is taken in all cases to be -99×10^{-6} emu/mol.[15,21] Second, we take the anisotropy of the spin paramagnetic part to be $\chi_c^s(T)/\chi_{ab}^s(T)=1.235$ as given by the data in Ref. 34 (see Sec. II C). This value is adopted for all compositions, following from our assumption that the g-factor anisotropy is independent of doping. Finally, the anisotropy of the orbital term is taken to be slightly greater than the factor of 4 dictated by the matrix elements, i.e., $\chi_c^{vv}/\chi_{ab}^{vv}\simeq4.5$, owing to the slightly larger energy denominator for χ_{ab}^{vv}.[45] The foregoing anisotropy relations, plus the two equations

$$\chi_\alpha^s(T)+\chi_\alpha^{vv}=\chi_\alpha^{expt}(T)-\chi_{dia}, \tag{13}$$

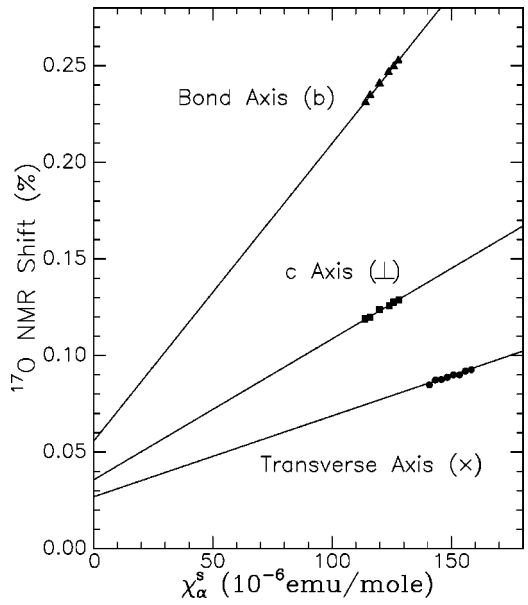

FIG. 4. The ^{17}O NMR shift data for planar sites with all three axis orientations are plotted here as a function of the corresponding spin susceptibility extracted from the experimental data (Ref. 32) as described in Sec. III E. The points shown correspond to 600 K $\leqslant T\leqslant$800 K. The solid lines are linear regressions. When extrapolated to $\chi_\alpha^s\rightarrow0$, these lines make positive intercepts yielding estimates of the chemical shift tensor components. See the text for further interpretation and error estimates.

$\alpha=c$ and ab, can then be solved for $\chi_\alpha^s(T)$ and χ_α^{vv}. The experimental data for several cases are listed in Table IV (Refs. 16, 21, 34, 46) along with the results of the spin-orbital partitioning procedure. The bottom entry in the table shows the high-field data from WCSG. χ_α^{vv} in the latter case is seen to be substantially larger than for the other three cases, where one finds $\chi_c^{vv}=52\pm7\times10^{-6}$ emu/mol. We suggest that the raw WCSG data are valid, but the analysis may be in error.[47] We observe also that the Van Vleck terms are roughly independent of doping level, as has been found in the case of YBCO.[48] Henceforth we shall adopt the values shown in the top line of Table IV.

The orbital susceptibilities in Table IV also have implications for conclusions reached in earlier work. In particular, the HF tensor for $La_{1.85}Sr_{0.15}CuO_4$ in Ref. 21 needs revision, because we now see that the orbital terms were overestimated, leading in turn to an overestimate of the HF tensor values. The doped LCO tensor components ($C_{d\alpha}$, $C_{d\alpha}^{an}$ listed in Table I) have been adjusted by combining the χ_α^{vv} values in Table IV with the experimental data in Ref. 21. The change in $C_{d\alpha}$ is $\sim-10\%$.

F. Estimate of chemical shifts

In Fig. 4 we plot the NMR shift tensor components (see Fig. 3) against the corresponding components of spin susceptibility $\chi_\alpha^s(T)=\chi_\alpha^{expt}(T)-\chi_{dia}-\chi_\alpha^{vv}$, where for $\chi_\alpha^{expt}(T)$ we adopt a linear regression fit to the data of Ref. 34 over the temperature range 500 K$\leqslant T\leqslant$800 K. As in Sec. III E, we

take $\chi_{dia} = -99 \times 10^{-6}$ emu/mol, and the values of χ_α^{vv} are taken from the first line of Table IV. For each orientation, the data in Fig. 4 exhibit the linear relationship already employed in Sec. II C to measure the shift coefficients, etc. Here, however, we run a linear regression for each plot. These lines, when extrapolated to $\chi_\alpha^s(T) \rightarrow 0$, yield an experimental estimate of the background ''chemical'' shift K_α^{orb}. The resulting K_α^{orb} tensor components, along with (2 standard deviation) error estimates, are listed in Table I. Chemical shifts are seen to vary from $\sim \frac{1}{4}$ to $\sim \frac{1}{3}$ of the total shift in the temperature range studied. Although the *a* and *c* axis values are equal within error limits, the bond (*b*) axis value is larger by a barely resolved margin. Interestingly, ^{17}O chemical shift values for YBCO (Ref. 31) also show a predominant bond axis component of similar magnitude, with smaller components along the other two axes. The two shift tensors are compared in Table I, where they are seen to agree within estimated errors.

One can formulate a perturbation theoretical estimate of the ^{17}O chemical shift contribution from the hybridized $3d$ holes, which produce the Van Vleck shift and susceptibility contributions on the copper ions. The same second-order formulas[27] that give rise to the corrections $\propto f_{SO}$ in Eqs. (6)–(8) can be shown to yield ''local'' terms for the vicinity of each ligand ion. We shall not describe such terms in detail, but only point out the inability of this approach to give results that resemble the experimental values in Table IV. The point here is that matrix elements of angular momentum that drive these terms will always vanish along the bond axis, where the dominant experimental contribution is found. The correct theory must therefore be a good deal more complex that this simple physical model based on an impurity state.

IV. CONCLUSIONS AND DISCUSSION

The anisotropic HF tensor of the planar ^{17}O has been interpreted in detail in terms of hybridization between the Cu $3d$ and O $2p_\sigma$ orbitals, which is also combined with mobile (oxygen $2p_\sigma$) hole density for the doped case as well. The measured covalency is in good agreement with the DF calculations of HSSM. At this level of covalency, some 31% of the spin density resides on the planar oxygen sites. Given a bit of hybridization with the apical O^{2-} as well, this means that barely 2/3 of the spin density resides on the copper sites. The bond axis anisotropy of the HF tensor is surprisingly large. Although some anisotropy in the sense observed is allowed by second-order spin-orbit coupling effects, the calculated effect is only about one-third of that observed. Attempts to interpret this result in terms of hybridization effects with the La^{3+} have not resulted in any firm conclusion. The latter effects were suggested by an unusually large range of NMR shifts reported earlier for the ^{139}La NMR.[16] Experimental data of somewhat greater accuracy would be required to convincingly resolve these questions. However, DF calculations[40] also show some HF anisotropy in the sense observed, and appear to account marginally for the data.

As for the isotropic HF interaction, the HSSM DF result is, in contrast, larger by 60% than the measured value for undoped La_2CuO_4. The mechanism for this effect is not revealed by the HSSM calculation, but one can only imagine that it is dominated by a $2s$ admixture to the hybridized HOMO wave function. Any core-polarization effect for the planar oxygens would undoubtedly be negative.[42] Thus, such an effect may account for the discrepancy between the HSSM calculations and the measured results, but not for the large, positive isotropic shift.

The increase of C^{iso} with doping (Table I) is also $\sim 60\%$. We consider this increase to be consistent, within errors, with the finding from the EFG results (see below) of 80% mobility for the doped holes in $La_{1.85}Sr_{0.15}CuO_4$. The latter would correspond to a 39% increase with doping of the hole density on the planar oxygens. It would be proportional to the number of Cu neighbors in the cluster calculations of HSSM[25] and therefore to the hole occupancy level on the oxygens in general. Such behavior would be expected of a $2s$ orbital admixture. It is interesting to make a rough estimate of the actual $2s$ admixture required to account for these effects. Using a recently calculated estimate $A_{2s} \sim 7000$ kG/spin for the $2s$ HF field (Ref. 49) of O^{2-}, we find $f_s \sim 0.007$. This seems like a reasonable number, since it is an order of magnitude smaller than the p_σ admixture deduced in Sec. IIIB. In contrast, there appears to be very little change or even a decrease in the anisotropic HF tensor with doping.[21] In this case the error limits are rather larger, and we suggest that no conclusion about the mobile charge density can be drawn from the latter result. A rather more quantitative picture is offered by the EFG tensor results.

The EFG tensor data presented here for LCO appears to be of good accuracy, as do the literature data for the doped case.[33] We have sought to interpret the changes with doping in terms of charge rearrangement in the crystal lattice, namely, the appearance of mobile hole density on the planar oxygens. A two-component model similar to that used by Takigawa *et al.*[31] to interpret the ^{17}O EFG, results in YBCO and leads to the satisfactory conclusion that $\sim 80\%$ of the doped holes are mobile, thus yielding a quantitative measure of the carrier level in the doped system. There are several aspects of this picture that merit comment. First, the agreement with the HSSM result is not good, the on-site component being well under half of the HSSM result, which is also local in character. On the other hand, more recent results from this group[40] exhibit the remarkable feature that the EFG tensor component arising from $2p_\sigma$ hole density has substantial axial anisotropy around the bond axis. This new effect, incorporated into our model, is important to the quality of the fit. It also prevented the admixture parameters ξ_{loc} and ξ_∞ from becoming unphysically small and large, respectively. How such effects play out in other compounds remains to be investigated.

The dramatic ^{17}O HF tensor anomaly, which occurs as one approaches T_N, remains unexplained up to now. Our earlier suggestion[16] that the extraordinarily large NMR shifts observed can only be understood in terms of $2s$ contact with HF couplings, is supported by the findings of the present paper. Now that the fundamental HF tensor contributions for this system are known, one can see that the $2p_\sigma$ HF coefficients would lead to oxygen spin-polarization levels an order of magnitude larger than the total measured values. Such a

result would be clearly unphysical. Even with the recently calculated $2s$ HF coeffiecient,[49] the oxygen site polarization is remarkably large, being -12% of the experimental value per formula unit. Thus, a surprising mechanism is at work here in any case. It remains an open question as to how such a mechanism comes into play in other systems, both in the published literature and in future investigations. Needless to say, efforts to identify the theoretical basis for these effects would be most welcome.

On the other hand, our understanding of the relaxation anomalies reported earlier[21–23] is not greatly improved by the relatively straightforward findings of the present paper. However, the anomalies in question appear to be consistent with the suggestion that dynamic magnetic stripe fluctuations occur in doped, superconducting LCO. The physical picture, in that case, would be that the fluctuation rate of stripe ordering lies somewhere between NMR frequencies and the lowest energies of inelastic neutron studies that show incommensurate peaks in the dynamic susceptibility.[17–19] The NMR dynamics therefore only ''see'' commensurate fluctuations, for which the transferred HF relaxation effects are unmeasurably small. The implication of this is that stripe fluctuations are responsible for the incommensurability of $\chi(\boldsymbol{q},\omega)$.[50] The degree of incommensurability observed for $\chi(\boldsymbol{q},\omega)$ is a measure of the spatial scale of the stripes. The fluctiation rate of such stripes remains an interesting question for investigation.

ACKNOWLEDGMENTS

The authors wish to thank the members (HSSM) of the University of Zurich theory group, and especially P.F. Meier, for extensive discussion of their results prior to publication.

*Present address: Advanced Science Research Center, Japan Atomic Energy Research Institute, Tokai-mura, Ibaraki-ken 319-1195, Japan.

[1] R.J. Cava, R.B. van Dover, B. Batlogg, and E.A. Rietman, Phys. Rev. Lett. **58**, 408 (1987).

[2] R.J. Birgeneau and G. Shirane, in *Physical Properties of High Temperature Superconductors*, edited by D. M. Ginsberg (World Scientific, Singapore, 1989).

[3] D.C. Johnston, J.P. Stokes, D.P. Goshorn, and J.T. Lewandowski, Phys. Rev. B **36**, 4007 (1987).

[4] S-W. Cheong *et al.*, Solid State Commun. **65**, 111 (1987); S-W. Cheong, J.D. Thompson, and Z. Fisk, Phys. Rev. B **39**, 4395 (1989).

[5] T. Thio, T.R. Thurston, N.W. Preyer, P.J. Picone, M.A. Kastner, H.P. Jenssen, D.R. Gabbe, C.Y. Chen, R.J. Birgeneau, and A. Aharony, Phys. Rev. B **38**, 905 (1988).

[6] T. Thio, C.Y. Chen, B.S. Freer, D.R. Gabbe, H.P. Jenssen, M.A. Kastner, P.J. Picone, N.W. Preyer, and R.J. Birgeneau, Phys. Rev. B **41**, 231 (1990).

[7] B. Keimer, A. Aharony, A. Auerbach, R.J. Birgeneau, A. Cassanho, Y. Endoh, R.W. Erwin, M.A. Kastner, and G. Shirane, Phys. Rev. B **45**, 7430 (1992); **46**, 14 034 (1992).

[8] T. Imai, C.P. Slichter, K. Yoshimura, and K. Kosuge, Phys. Rev. Lett. **70**, 1002 (1993).

[9] M. Matsumura *et al.*, J. Phys. Soc. Jpn. **63**, 4331 (1994).

[10] S. Chakravarty, B.I. Halperin, and D.R. Nelson, Phys. Rev. Lett. **60**, 1057 (1989); S. Tyc, B.I. Halperin, and S. Chakravarty, *ibid.* **62**, 835 (1989); S. Chakravarty, B. I. Halperin, and D. R. Nelson, Phys. Rev. B **39**, 2344 (1989).

[11] L.L. Miller, X.L. Wang, S.X. Wang, C. Stassis, D.C. Johnston, J. Faber, Jr., and C.-K. Loong, Phys. Rev. B **41**, 1921 (1990); D. Vaknin, S.K. Sinha, C. Stassis, L.L. Miller, and D.C. Johnston, *ibid.* **41**, 1926 (1990).

[12] I. Dzyaloshinski, J. Phys. Chem. Solids **4**, 241 (1958); T. Moriya, Phys. Rev. **120**, 91 (1960).

[13] K.R. Thurber, A.W. Hunt, T. Imai, F.C. Chou, and Y. Lee, Phys. Rev. Lett. **79**, 171 (1997).

[14] D. Coffey, K.S. Bedell, and S.A. Trugman, Phys. Rev. B **42**, 6509 (1990); D. Coffey, T.M. Rice, and F.C. Zhang, *ibid.* **44**, 10 112 (1991).

[15] T. Thio and A. Aharony, Phys. Rev. Lett. **73**, 894 (1994).

[16] R.E. Walstedt, S-W. Cheong, J. Sunstrom, and M. Greenblatt, Phys. Rev. Lett. **80**, 2457 (1998).

[17] S-W. Cheong, G. Aeppli, T.E. Mason, H. Mook, S.M. Hayden, P.C. Canfield, Z. Fisk, K.N. Clausen, and J.L. Martinez, Phys. Rev. Lett. **67**, 1791 (1991); T.E. Mason, G. Aeppli, and H. Mook, *ibid.* **68**, 1414 (1992).

[18] M. Matsuda, K. Yamada, Y. Endoh, T.R. Thurston, G. Shirane, R.J. Birgeneau, M.A. Kastner, I. Tanaka, and H. Kojima, Phys. Rev. B **49**, 6958 (1993).

[19] G. Aeppli, T.E. Mason, S.M. Hayden, H.A. Mook, and J. Kulda, Science **278**, 1432 (1997).

[20] R.M. White, *Quantum Theory of Magnetism*, Springer Series in Solid-State Sciences Vol. 32, edited by M. Cardona, P. Fulde, and H.-J. Queisser (Springer-Verlag, New York, 1983).

[21] R.E. Walstedt, S. Shastry, and S-W. Cheong, Phys. Rev. Lett. **72**, 3610 (1994).

[22] R.E. Walstedt, J. Phys. Chem. Solids **59**, 2155 (1998).

[23] R.E. Walstedt and S-W. Cheong, Phys. Rev. B **51**, 3163 (1995).

[24] B.S. Shastry, Phys. Rev. Lett. **63**, 1288 (1989).

[25] P. Hüsser, H.U. Suter, E.P. Stoll, and P.F. Meier, Phys. Rev. B **61**, 1567 (2000).

[26] F.C. Zhang and T.M. Rice, Phys. Rev. B **37**, 3759 (1988).

[27] A. Abragam and B. Bleaney, *Electron Paramagnetic Resonance of Paramagnetic Ions* (Clarendon, Oxford, 1970), Chap. 20.

[28] There is a difference of $\sim 15\%$ between the T_1 values of the two copper isotopes, as well as a small variation from site to site of the spin-spin couplings with differing isotopic composition of Cu neighbor spins. These effects give rise to a narrow distribution of T_2 values, which would be observable only with extraordinarily precise data.

[29] A. Abragam, *The Principles of Nuclear Magnetism* (Oxford University, Oxford, 1961).

[30] T. Imai *et al.*, J. Phys. Soc. Jpn. **59**, 3846 (1990).

[31] M. Takigawa *et al.*, Phys. Rev. Lett. **63**, 1865 (1989).

[32] In this notation, b represents the bond axis, a the in-plane transverse axis, and c the axis perpendicular to the CuO_2 planes.

[33] K. Ishida, U. Kitaoka, G. Zheng, and K. Asayama, J. Phys. Soc. Jpn. **60**, 3516 (1991); G. Zheng *et al.*, *ibid.* **64**, 2524 (1995).

[34] D.C. Johnston *et al.*, in *Electronic Properties and Mechanisms of High T_c Superconductors*, edited by T. Oguchi, K. Kadowaki,

and T. Sasaki (Elsevier Science, B.V., Amsterdam, 1992), p. 301.

[35] With the HF constant defined as given in the text, the HF field per unit of spin is $C_\alpha/\gamma_{17}\hbar$. In units of kG/μ_B, the HF constant is $C_\alpha/g_\alpha\gamma_{17}\hbar$, i.e., smaller by the factor g_α.

[36] For simplicity, we have collapsed the crystal-field splitting parameters Δ_0 (xy) and Δ_1 $(yz$ and $zx)$ into a single parameter Δ. See Ref. (AB) for details.

[37] See AB, Table 24, p. 877.

[38] If λ_p and λ_t are the admixture coefficients for the ground p_σ and excited p_π orbitals, respectively, then $f_{p\sigma}=\frac{1}{4}\lambda_p^2 N_\sigma^{-1}$ and $f_p'=\frac{1}{4}\lambda_p\lambda_t(N_\sigma N_t)^{-(1/2)}$.

[39] See AB, Chap. 20 for details.

[40] E.P. Stoll *et al.* (unpublished).

[41] K. Hanzawa, F. Komatsu, and K. Yosida, J. Phys. Soc. Jpn. **59**, 3345 (1990).

[42] R.E. Watson and A.J. Freeman, in *Hyperfine Interactions*, edited by A.J. Freeman and R.J. Frankel (Academic, New York, 1967), p. 53.

[43] M.H. Cohen and F. Reif, *Solid State Physics*, edited by F. Seitz and D. Turnbull (Academic, New York, 1957), Vol. 5.

[44] P.C. Hammel, B.W. Statt, R.L. Martin, F.C. Chou, D.C. Johnston, and S-W. Cheong, Phys. Rev. B **57**, R712 (1998).

[45] See Ref. 27, p. 456.

[46] I. Terasaki *et al.*, Physica C **193**, 365 (1992).

[47] In retrospect, the assumption in Ref. 16 that $\chi_c^s(T)/\chi_{ab}^s=(g_c/g_{ab})^2$, may be incorrect near the ordered phase, because the spin-flop effect occurs for one field orientation but not the other.

[48] R.E. Walstedt, W.W. Warren, Jr., R.F. Bell, R.J. Cava, G.P. Espinosa, L.F. Schneemeyer, and J.V. Waszcak, Phys. Rev. B **41**, 9574 (1990).

[49] P.F. Meier (private communication).

[50] J.M. Tranquada, J.D. Axe, N. Ichikawa, A.R. Moodenbaugh, Y. Nakamura, and S. Uchida, Phys. Rev. Lett. **78**, 338 (1997) and references therein.